Photofragmentation of the Fluorene Cation: II. Determination of the H-Loss Energy-Dependent Rate Constant

Nguyen-Thi Van-Oanh,*,† Pierre Désesquelles,‡ and Philippe Bréchignac†

Laboratoire de Photophysique Moléculaire, CNRS, Fédération de Recherche Lumière Matière, Bât 210, Université Paris-Sud XI, F91405 Orsay Cédex, France, and Institut de Physique Nucléaire, IN2P3, Bât 100, Université Paris-Sud XI, F91405 Orsay Cédex, France

Received: December 8, 2005; In Final Form: February 28, 2006

The hydrogen-loss channel, induced by sequential multiphoton absorption, of the vapor-phase fluorene cation was investigated using a pulsed supersonic molecular beam, a time-of-flight mass spectrometer, and pulsed nanosecond lasers. Our new method leads to the determination of the absolute absorption cross section. Its attenuation with the number of absorbed photons has been approximated by means of statistical models. A model-free determination of the evolution of the dissociation rate constant in a relatively large energy range was obtained by solving the set of coupled differential kinetic equations numerically. Particular attention was focused on the data analysis techniques. The free fit of these rate constants is close to the photothermodissociation statistical model, but shows a discrepancy with the Rice and Ramsperger and Kassel model mainly at high energy. The resulting activation energy is in agreement with both that deduced from the ab initio calculations and that from the tight-binding energy potential surface model.

Introduction

In unimolecular reactions, the dissociation rate constant is a fundamental parameter of the activated system. We will focus more specifically on the dissociation mechanism, within a wide energy range, of the polycyclic aromatic hydrocarbons (PAHs) energetically excited by photoabsorption. Indeed, PAHs could be responsible for the emission of characteristic infrared bands observed in the interstellar medium.[1−3] To validate this conjecture, one has to study the competition between fragmentation and IR emission. In this paper, we characterize the evolution of the rate constant of the H-loss channel, as a function of energy deposit, in this kind of species. Astrophysical observations suggest that parts of the interstellar PAHs could be made of cations and of molecules including a pentagonal ring.[4,5] For these reasons, and because of its availability in a suitable form for laboratory experiments, we have chosen to study the fragmentation of the fluorene cation ($C_{13}H_{10}^+$).

The full experimental determination of the energy dependence of the rate constant for large molecules in a wide energy range is difficult. These experiments are limited to rather narrow energy ranges.[6−11] Moreover, most experimental methods of determination of the energy-dependent dissociation rates depend strongly on statistical models whose parameters are adjusted to the measurements. The classical Rice, Ramsperger, and Kassel (RRK) model[12,13] is usually employed to give a rough picture of the activation function. Its semiclassical version, in which the zero point energy is accounted for, has been proposed recently by Léger and co-workers.[14] This model is often termed the "photothermodissociation" (PTD) model. In addition, it is well known that the way the dissociation rate evolves with internal energy varies from one model to another. Consequently, it is important to be able to perform the data analysis without necessarily introducing any statistical model, particularly, in order for the theoretical models to be validated. It has to be noted that some rigorous and sophisticated calculations, regarding the dissociation rate determination of the related aromatic molecules, are also found in the literature.[15−18]

In a previous work,[19] we have focused on our new experimental procedure, which is sensitive to the evolution of the dissociation rate over a wide energy range. The method is conceived for fixed time-of-flight mass spectroscopy experiments but is also adaptable for reflection spectrometers. The experimental setup and the features of the detected fragmentation mass spectra whose data are under study here are described in the previous paper.[19] A beam of fluorene cations was obtained using a seeded supersonic molecular beam and one-color two-photon ionization. These *parent* molecules were excited via sequential photon absorptions from a nanosecond laser ($h\nu$ = 1.97 and 3.4 eV). The fragmentation products were identified using a time-of-flight mass spectrometer. The mean number of absorbed photons was tuned by varying the laser flux. It has been shown[19] that the absorption phase is not Poissonian, at least at medium and high photon fluxes. This has been interpreted[19] as an indication that fragmentation takes place during the laser pulse and, as will be seen in the following, that the absorption cross section may vary with the number of absorbed photons.

In this paper, we will introduce the transition matrix method, which allows one to handle complex experimental dissociation schemes including, for example, absorption/fragmentation competition. This analysis will result in the determination of the dissociation paths. Using the RRK and PTD hypotheses, we then determine the evolution of the absorption cross section of the fluorene cation with the number of absorbed photons. Finally, we perform a model-free determination of the H-loss dissociation constant as a function of the energy deposited. Only the outline of the analysis is developed in the text; technical details can be found in the appendices.

* Corresponding author. E-mail: vanoanh@lcp.u-psud.fr. Present address: Laboratoire de Chimie Physique, UMR 8000, CNRS, Bât 349, Université Paris-Sud XI, F91405 Orsay Cédex, France.

† Laboratoire de Photophysique Moléculaire.

‡ Institut de Physique Nucléaire.

10.1021/jp057168x CCC: $33.50
Published on Web 04/01/2006

Transition Matrix Method

In this section, we introduce a very general method for determining the dissociation constants as well as the absorption constants. This method is still valid in the cases when absorption and fragmentation are in competition.[20] It takes advantage of the fact that the molecular population evolutions are Markovian processes in the sense that the populations at time $t + \mathrm{d}t$ depend only on the populations at time t and on constant parameters (absorption/dissociation constants).

We consider a very general decay scheme in which the parent fluorene cations can absorb an unlimited number of photons and break up by hydrogen-loss or by other fragmentation yields referred to as *leak*. The evolution of the molecular population after a small time interval is given by: $\mathbf{N}(t + \Delta t) = \mathbf{N}(t) + \Delta\mathbf{N}$ where $\mathbf{N}$ is the column vector of the molecular population:

$$\mathbf{N} = \begin{pmatrix} N_{-\mathrm{H}} \\ N_{\mathrm{leak}} \\ N_{\mathrm{p}}^{0*} \\ \vdots \\ N_{\mathrm{p}}^{j*} \\ \vdots \end{pmatrix} \tag{1}$$

N_{p}^{j*} being the proportion of parent molecules having absorbed j photons, $N_{-\mathrm{H}}$ being the H-loss yield, and N_{leak} being the leak yield. Using the kinetic equations, one obtains

$$N_{-\mathrm{H}}(t + \Delta t) = N_{-\mathrm{H}}(t) + \sum_j k_{-\mathrm{H}}^{j*}\,\Delta t\, N_{\mathrm{p}}^{j*}$$

$$N_{\mathrm{leak}}(t + \Delta t) = N_{\mathrm{leak}}(t) + \sum_j k_{\mathrm{leak}}^{j*}\,\Delta t\, N_{\mathrm{p}}^{j*}$$

$$N_{\mathrm{p}}^{0*}(t + \Delta t) = (1 - k_{\mathrm{abs}}^{1*}\,\Delta t)\, N_{\mathrm{p}}^{0*}(t)$$

$$N_{\mathrm{p}}^{j*}(t + \Delta t) = k_{\mathrm{abs}}^{j-1*}\,\Delta t\, N_{\mathrm{p}}^{j-1*}(t) + [1 - (k_{\mathrm{abs}}^{j+1*} + k_{-\mathrm{H}}^{j*} + k_{\mathrm{leak}}^{j*})\Delta t]\, N_{\mathrm{p}}^{j*}(t) \tag{2}$$

where k_{abs}^{j*} is the photon absorption rate constant of the jth photon and $k_{-\mathrm{H}}^{j*}$ and k_{leak}^{j*} are the rate constants for the H-loss and leak channels. The previous system can be written as

$$\mathbf{N}(t + \Delta t) = \mathscr{T}\,\mathbf{N}(t) \tag{3}$$

where $\mathscr{T}$ is the transition matrix of the molecular populations. It can be written as: $\mathscr{T} = \mathbf{1} + (\mathscr{K} - \mathscr{D}_{\mathscr{K}})\Delta t$, where $\mathbf{1}$ is the unit matrix, $\mathscr{K}$ is the rate constant matrix, and $\mathscr{D}_{\mathscr{K}}$ is the diagonal matrix whose elements are equal to the sum of the corresponding column of the latter matrix. The elements of the rate constant matrix are equal to the rate constant of the transformation of the jth column molecule into the ith line molecule. For example, in the case of the left scheme of Figure 1, the rate constant matrix reads

$$\mathscr{K} = \begin{pmatrix} 0 & 0 & 0 & k_{-\mathrm{H}}^{1*} & k_{-\mathrm{H}}^{2*} & k_{-\mathrm{H}}^{3*} & k_{-\mathrm{H}}^{4*} & k_{-\mathrm{H}}^{5*} \\ 0 & 0 & 0 & 0 & 0 & 0 & 0 & k_{\mathrm{leak}}^{5*} \\ 0 & 0 & 0 & 0 & 0 & 0 & 0 & 0 \\ 0 & 0 & k_{\mathrm{abs}}^{1*} & 0 & 0 & 0 & 0 & 0 \\ 0 & 0 & 0 & k_{\mathrm{abs}}^{2*} & 0 & 0 & 0 & 0 \\ 0 & 0 & 0 & 0 & k_{\mathrm{abs}}^{3*} & 0 & 0 & 0 \\ 0 & 0 & 0 & 0 & 0 & k_{\mathrm{abs}}^{4*} & 0 & 0 \\ 0 & 0 & 0 & 0 & 0 & 0 & k_{\mathrm{abs}}^{5*} & 0 \end{pmatrix} \tag{4}$$

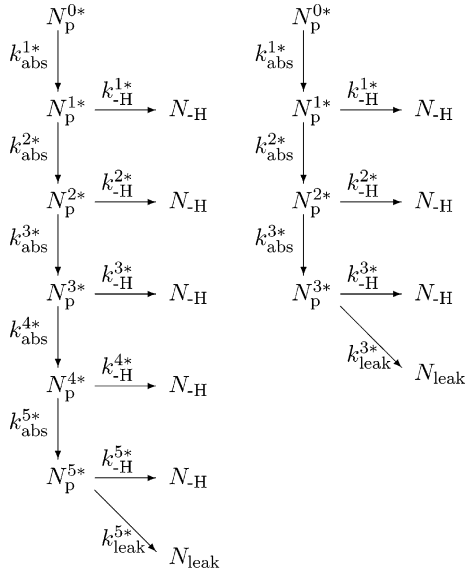

Figure 1. Dissociation schemes of the fluorene cation by hydrogen loss. The left scheme corresponds to 1.97 eV photons and the right one to 3.4 eV photons.

A modification in the absorption and fragmentation scheme is taken into account merely by a modification of this matrix.[21] With n as the number of time steps, we have

$$\mathbf{N}(t_{\mathrm{final}}) = \mathscr{T}^n\,\mathbf{N}(t_0) \tag{5}$$

This equation allows one to calculate[22] the molecular populations at a final time knowing the population at an initial time ($\mathbf{N}(t_0)$: (0, 0, 1, 0,..., 0)).

We have to consider two transition matrices. The first one corresponds to the irradiation phase. The second matrix, associated with the flight from the end of the laser pulse to the end of the acceleration zone of the spectrometer, is equal to the former one except that all absorption constants are set equal to zero.

This method was used to calculate the optimum values of the dissociation constants using a minimization algorithm.[23] The minimization criterion is the weighted chi-square between the experimental molecular proportions and the proportions given by eq 5.

Dissociation Scheme

The experimental evolutions of the $N_{-\mathrm{H}}$ and N_{leak} proportions, as a function of the laser intensity (Figure 3), show some concavity changes. It is not possible to reproduce these shapes if the maximum number of absorbed photons is strictly lower than 5 for the 1.97 eV experiment and 3 for the 3.4 eV experiment. Thus, these numbers will be fixed to these two values. The coherence of the results will be checked at the end of the analysis (Appendix C). In both cases, the leak threshold is such that leak appears only for the maximum number of absorbed photons.

For the first experiment, as was shown in the previous paper,[19] we have to consider, in the kinetic model, the evolution of the cross section with internal energy and the fragmentation/absorption competition during the irradiation time. If no absorption cross-section attenuation was considered, then it would not be possible to reproduce simultaneously the rapid increase of the hydrogen-loss yield at low intensity and its saturation at medium energy. Thus, the absorption constant depends on the number of absorbed photons. At this point, the

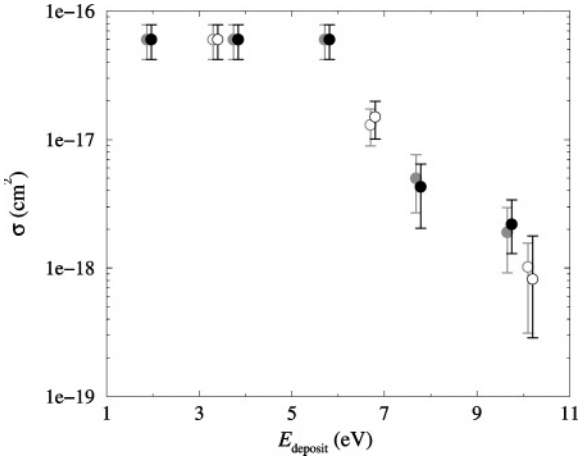

Figure 2. Evolution of the absorption cross section of 1.97 eV (dots) and 3.4 eV (open dots) photons by the fluorene cation as a function of the energy deposit. The black symbols correspond to the adjustments performed using the PTD law, and gray symbols correspond to the adjustments performed using the RRK law (these points were shifted slightly to the left for better readability).

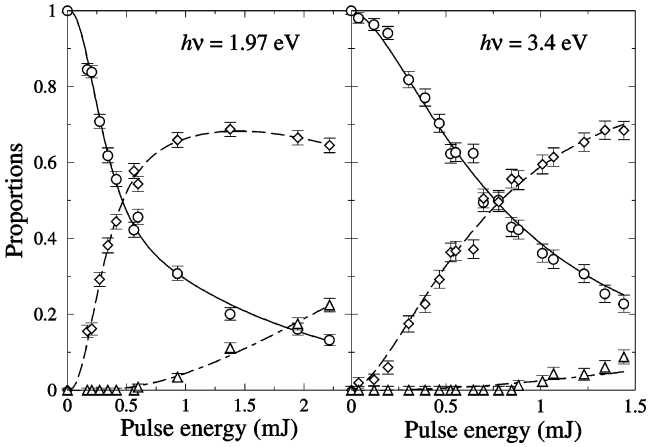

Figure 3. Comparison of the experimental proportions (circles: parent molecules, diamonds: hydrogen loss, triangles: leak) with the theoretical results (lines) obtained by the free adjustment (see text) considering the decreasing absorption cross section for the hot fluorene shown in the previous figure.

number of adjustable parameters would be 10 for the former experiment and 6 for the latter, which is too large with respect to the number of experimental measurements. In order to both lower the number of parameters and confront these statistical laws with the experimental data, the dissociation constant was first constrained to follow successively the RRK and the PTD evolutions, which are characterized by two parameters noted E_0 and k_0

$$k_{-\mathrm{H}}^{j^*} = k_0\left(1 - \frac{E_0}{jh\nu}\right)^{g-1} \quad \text{RRK} \tag{6}$$

$$k_{-\mathrm{H}}^{j^*} = k_0\left(1 - \frac{E_0}{jh\nu + E_{\mathrm{zp}}}\right)^{g-1} \quad \text{PTD} \tag{7}$$

where $g = 63$ is the number of degrees of freedom of the fluorene cation and $E_{\mathrm{zp}} = 7.4$ eV is its zero point energy (this value was obtained from a tight-binding model[24]). The parameters E_0 and k_0 can be understood as the activation energy and the characteristic carbon−hydrogen vibrational frequency, respectively. It will be seen below that only the minimum values of the leak constants are constrained by the experimental results.

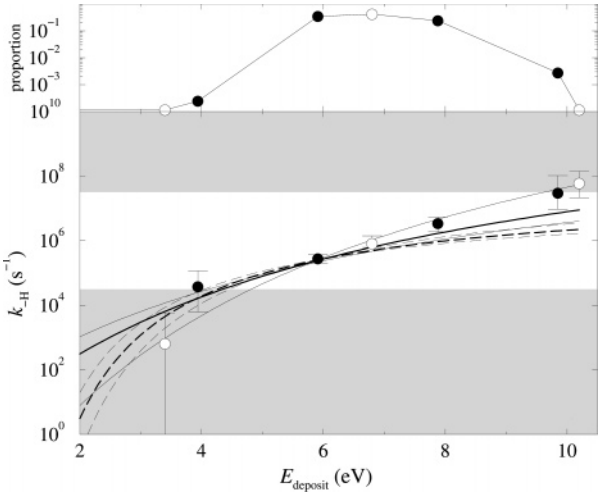

Figure 4. Evolution of the dissociation constant as a function of the energy deposit (bottom). The bold line corresponds to the assumption that $k_{-\mathrm{H}}$ follows the PTD law, the bold dashed line corresponds to the assumption that $k_{-\mathrm{H}}$ follows the RRK law, and the circles correspond to the free adjustment. The thin lines in the RRK and PTD cases indicate the uncertainties connected to the bivariate error contours of the E_0 and k_0 parameters. The black dots correspond to a photon energy of 1.97 eV, and the open dots correspond to a photon energy of 3.4 eV. The unshaded zone corresponds to the best sensitivity domain of the spectrometer. The curve at the top shows the proportion of parent molecule fragmentation as a function of the energy deposit (see text).

Moreover, for the 1.97 eV experiment, the attenuations of the cross section after the absorption of one or two photons are negligible; thus, they have been removed from the analysis. Finally, the number of adjustable parameters is reduced to two excited-molecule cross sections for each experiment plus the common E_0 and k_0 parameters. The absorption and dissociation schemes are shown in Figure 1.

Results

When taking into account the saturation of the photon absorption with the energy deposited, the agreement of the adjustments with the experimental data becomes very good. The agreement is slightly better when the hydrogen-loss rate constant is constrained to follow the PTD law instead of the RRK law.

The evolution of the cross section with the energy deposited is shown in Figure 2. This figure shows that the resulting variations of $\sigma(E_{\mathrm{deposit}})$ are continuous and monotonic, the evolution is the same for both photon energies, and the variations of the cross section are almost the same for two different hypotheses on the statistical law followed by the dissociation coefficient.[25]

Hence, a new minimization (referred to in the following as *free* adjustment) was performed fixing the cross sections to the average values found in the preceding analyses. All of the dissociation constants are now treated as free parameters. The resulting reduced chi-square of the minimizations are 0.89 and 1.02. Thus, the agreement between the experiment and the results from this analysis is very good as shown in Figure 3.

The evolution of the dissociation constant with the energy deposited for the three minimizations is presented in Figure 4. In the RRK and PTD cases, the evolution behavior is different for small and large amounts of energy deposited. This is possible because the sensitivity of the experiment is low in these domains. This sensitivity is imposed by the experimental setup (see the best sensitivity zone of the spectrometer as calculated by our simulation code[26] in Figure 4) and by the dissociation scheme. This latter effect refers to the fact that the more parent molecules

that break up after absorption of a given number of photons the more precise the measurement of the corresponding rate constant. Using the time evolution calculation (see Appendix C) one can determine the distribution of energy deposited prior to fragmentation (see top of Figure 4). It is remarkable that the two criteria, which are only partly correlated, lead to the same optimum sensitivity energy domains. Thus, at low and high intensities, both effects play a role. At low energy deposit, the curves reach the lower limit of the spectrometer. These values of the rate constant could be accessible using the ion trap technique.[11,27,28]

Thus, the central part (from 3.5 up to 9 eV) of the figure is significant. In this zone, the value of the dissociation constants obtained by the different methods are very similar. In the cases of the RRK and PTD procedures, the uncertainty regions are indicated by thin lines (these uncertainties are obtained considering the extreme values of the error contour in the E_0, ln(k_0) plane, see Appendix B). The uncertainties are minimum at the center of the spectrometer sensitivity zone.

The value of the dissociation constant obtained using the free adjustment and the PTD adjustment are close. The only large discrepancy corresponds to the point associated with the absorption of two 1.97 eV photons. Close to the threshold the PTD law seems to overestimate the value of the dissociation rate constant.

The PTD procedure leads to an estimate of the dissociation threshold, E_0, of 2.62 eV and a k_0 constant of 2×10^{11} s^{-1}. The uncertainties play a particular role in these measurements. Indeed, the monovariate error bars (obtained considering that the other minimization parameters take the value corresponding to the optimum) are very small: about 3% for E_0 and ln k_0. Nevertheless, the smallness of these error bars is deceptive because of the very strong coupling between E_0 and k_0. Thus, it is necessary to consider the bivariate error contour of the pair of parameters. The uncertainties presented in Figure 4 have been calculated in this way. Now the relative uncertainties are large, 29% and 17%, respectively. These uncertainties are due partly to our experimental setup but are due mainly to the very forms of the statistical equations (see Appendix B). Hence, any experimental determination of the parameters of these statistical laws must be followed by a careful analysis of the bivariate uncertainties.

We notice that the ab initio theoretical value predicted by DFT/B3LYP using cc-pvdz is $E_0 = 2.6$ eV. A little difference can be seen due to the basis-set effect ($E_0 = 2.7$ eV using 6-31G-(d,p)[29]). The value obtained by our tight-binding molecular dynamics[24] is $E_0 = 2.1$ eV. Both are in agreement, within uncertainties, with the experimental determination.

Discussion and Conclusions

Absorption Cross Section. The absorption cross section for the cold fluorene cation has been determined in ref 30 ($\sigma \approx 0.6 \times 10^{-16}$ cm^{-2} at $\lambda = 630$ nm). This value is confirmed using our experimental data.[19] In this paper, we have determined that the absorption cross section decreases as a function of the energy deposited.

A new method for processing the data, based on the transition matrix, was introduced. This method allows one to test different hypotheses on the absortion/fragmentation process easily and determine the evolution of the rate constants as a function of the deposit energy.

The evolution of the absorption cross section with the number of photons was first determined imposing the RRK and PTD laws. Both adjustments reproduce the experimental data satisfactorily. It is remarkable that the minimization procedures result in monotonic evolutions of the cross section, which are very similar for both statistical laws.

TABLE 1: Numerical Values of the H-Loss Rate Constants as a Function of the Deposit Energy for the Free Adjustment (Same as Figure 4)[a]

$E_{deposit}$	k_{-H}	k_{-H}^{min}	k_{-H}^{max}
3.40	6.5×10^2	0	5.2×10^3
3.94	3.7×10^4	5.8×10^3	1.1×10^5
5.91	2.8×10^5	1.8×10^5	3.3×10^5
6.80	8.2×10^5	5.7×10^5	1.3×10^6
7.88	3.1×10^6	1.7×10^6	5.3×10^6
9.85	3.0×10^7	8.8×10^6	9.1×10^7
10.20	6.0×10^7	2.1×10^7	1.3×10^8

[a] The energy is given in eV and the rate constants are given in s^{-1}.

Finally, the constant rates were treated as free parameters. The resulting variations of the molecule populations reproduce the experimental data very closely. The variations of the $k_{-H}(E_{deposit})$ appear to be very similar to the evolution found under the PTD hypothesis, except in the region close to the threshold. We consider the results given by the free adjustment as the most reliable.

Dissociation Scheme. The main features of the dissociation scheme have been presented already in the above discussion. During the irradiation phase, absorption competes with fragmentation mostly at high laser intensity. The time evolution plots (Appendix B) show that the only fragmentation channel open during the acceleration phase is the hydrogen loss. The other fragmentation channels occur only during the irradiation phase. The saturation of the photon absorption is explained both by this competition and by the attenuation of the absorption cross section with the energy deposited. Using the transition matrix we have shown that, to reproduce the different molecular proportion concavity changes, it was necessary to take into account up to five absorbed photons for the first experiment and three for the second. The fact that this number is lower for the second experiment does not come as a surprise because at given E_{laser} and t_{pulse}, the absorption probability is proportional to σ/S and to $1/(h\nu)$. We have seen that the σ/S ratios were the same for the two experiments; thus, the ratio of the maximum numbers of absorbed photons for the two experiments must be close to the inverse ratio of the photon energies. In practice, the maximum energy deposited is the same for both experiments. The time evolution plots confirm that, when the maximum number of photons is reached, the fragmentation is too sudden to allow for extra photon absorptions.

Dissociation Rate Constants. The values of the dissociation constants, as obtained by the free adjustment taking into account the decrease of the absorption cross section, are given in Table 1.

The value of the dissociation constant obtained using the free adjustment and the PTD adjustment are close. The only large discrepancy corresponds to the point associated with the absorption of two 1.97 eV photons. Close to the threshold the PTD law seems to overestimate the value of the dissociation rate constant.

These values are compatible with the fragment appearance potential threshold measured in ref 31 ($E_{app} = 5.06$ eV) for which the authors give an estimate of the dissociation constant of 10^4 s^{-1}. Interpolating our results for this energy, it gives an approximate value of 9×10^4 s^{-1}.

We have verified one of the rate constants using our signal shape simulation code (Appendix C). This analysis gives a very good reproduction of the experimental signal shape, and the

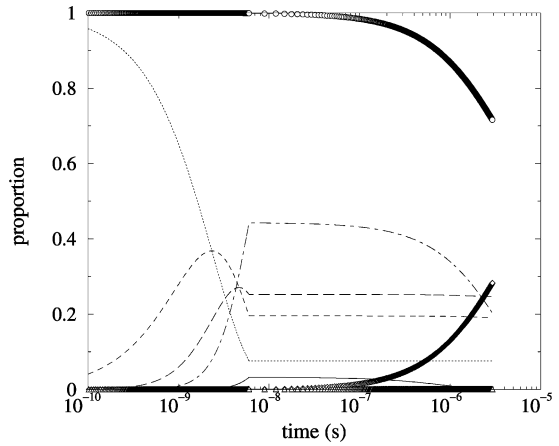

Figure 5. Simulated time-dependence of the parent and its products' populations at low intensity (1.97 eV, 0.27 mJ). The symbols stand for the molecules whose proportions are measured experimentally (circles: excited or stable fluorene$^+$, diamonds: H-loss channel, triangles: other fragmentation channels). The lines correspond to the different excitation levels of the fluorene$^+$ (dotted: not excited, dashed: absorption of one photon, long dashed: two photons, dotted−dashed: three photons, full: four photons).

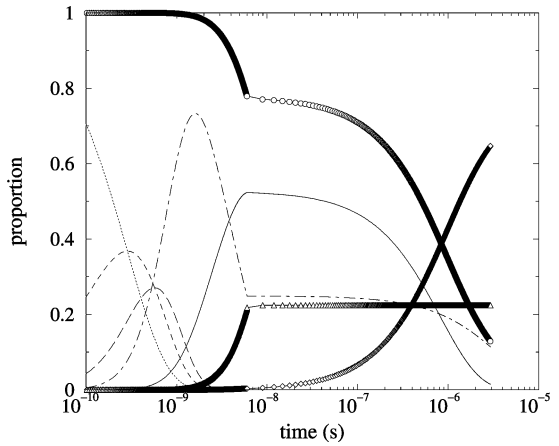

Figure 6. Time evolution of the population of the different kinds of molecules for a high laser intensity (1.97 eV, 2.2 mJ). Same conventions as for the previous figure.

resulting value of the rate constant is in good agreement with the one obtained by the transition matrix technique.

The values of the dissociation constant corresponding to the other fragmentation channels (k^{j*}_{leak}) have no real signification because, on one hand, they correspond to the overimposition of different channels and, on the other hand, only their minimum value is constrained.

According to the estimated IR emission rate, the rate constants obtained above and the estimated photon energy in space, the fluorene cation is likely not present the interstellar medium. If it was present, then it would be under the $C_{13}H_9$ fluorene-like radical because of its better stability.

Perspectives. We will apply this method that allows a direct determination of the evolution of rate constants as a function of deposited energy to several PAHs and also to the different fragmentation channels for further studies.

Furthermore, a rigorous theoretical treatment is currently carried out using a phase space theory, considering the anharmonic quantum density of states, developed in previous works.[32,33] This method is currently applied to the H-loss channel of the fluorene cation, and, more generally, seems very promising for the calculation of rate constants.

Appendix A: Time Evolution of the Molecular Populations

When the values of the absorption and fragmentation velocities are known, it is possible to visualize the evolution of the molecular populations as a function of time. To speak in a vivid way, the film of the dynamical mechanism can be unfolded from the pictures of the final states, that is, from the detector signals. This is done by calculating iteratively, using the transition matrix (eq 3), the vector containing the molecular populations (eq 1). The evolutions for two experimental points are presented in Figures 5 and 6. The left part of the figures, up to 6 ns, corresponds to the laser pulse, and the right part corresponds to the acceleration zone of the spectrometer. This section is meant to describe the absorption/fragmentation dynamics and validate some of the hypotheses made in the analysis.

Low Laser Intensity. Even at low laser intensity (Figure 5), only a small proportion of the parent molecules is submitted to the laser pulse without being excited. This shows the efficiency of this experimental setup for the heating of the molecules. In this figure, the different line types correspond to the different excitation levels. The curves related to the weakly excited molecules (two photons or less) show no variation after the laser pulse. In the two-photon case, this is because the inverse of the dissociation constant is very large with respect to the acceleration time. In the other cases, the internal energy is not sufficient to allow fragmentation. Only the molecules absorbing three photons have a rate constant large enough to lose an hydrogen atom. This explains the mirror evolutions of the dotted−dashed curve and of the diamond curve. At such a low intensity, the parent molecules do not break up during the pulse time and almost no molecule is excited over three photons; thus, the absorption process is Poissonian.

High Laser Intensity. Contrary to what happens at low intensity, the parent molecule proportion at high intensity decreases rapidly: as seen in Figure 6, a large part of the parent molecules is fragmented before the end of the laser pulse. The absorption process is no longer Poissonian.

This result illustrates the saturation of the absorption process. At high laser intensity, all of the parent molecules are excited, some molecules absorb up to five photons. The latter molecules break up immediately (because the values of $k^{5*}_{-\text{H}}$ and k^{5*}_{leak} are very high with respect to the inverse of the time-of-flight); thus, their proportion stays very small. Our hypothesis, namely, that the de-excitation scheme could be stopped at five photons, is thus strengthened. At the end of the laser pulse, all of the remaining parent molecules have absorbed three or four photons. The fragmentation will continue during the acceleration phase but is slowed because all of the five-times excited molecules have already undergone fragmentation. The four-times excited molecules will break up prior to detection. Thus, all of the detected parent molecules are excited by three photons. The leak curve keeps constant after the laser pulse because all of the five-times excited molecules have already fed this channel and the less excited molecules cannot break up in a way other than hydrogen loss.

Final Comments. At medium and high laser intensities, an important part of the fragmentation process takes place during the irradiation. Within this period of time, a complex competition process occurs between absorption and fragmentation. One cannot expect, for example, to be able to adjust the experimentally measured proportions with a simplified version of the kinetic law. This observation confirms the conclusion of the Poisson−Gauss analysis of ref 19.

Although the laser pulse is long enough to allow the fluorene cation to absorb in theory up to 20 photons, the fragmentation of molecules excited by absorbing more than four sequential photons is so rapid that the absorption of a sixth photon is very unlikely. We can conclude, on one hand, that the hypothesis that the dissociation scheme is stopped at five photons is validated, and, on the other hand, that the absorption process is limited more by fragmentation than by the irradiation time.

Depending on the length of the acceleration zone, the experiment is sensitive, or not, to different ranges of rate constants. However, important evolutions of the molecule populations can be seen inside the acceleration zone, as well for low intensities as for high intensities. This shows that this spectrometer was well adapted to the measurement of the fragmentation rate of the fluorene cation in the energy range of interest.

Appendix B: Errors on E_0 and k_0

The aim of this appendix is to show how the uncertainties on the statistical law parameters can be evaluated. The values of these uncertainties are connected to a given experimental setup, but they are also induced by the very form of the statistical laws. Hence, the following results and lines of thought can be useful in many experimental analyses. Our goal will also be to show how the values found for the one-dimension uncertainties may be deceptive because of the lengthening of the two-dimension error contour.

Uncertainties and the Statistical Laws. Most experiments aiming at evaluating the evolution of the dissociation rate constant consist, directly or, as in our case, indirectly, in measuring the values of k^{j*} for several values of the number j of absorbed photons. The resulting unnormalized χ^2 reads (for the sake of simplicity the χ^2 is applied to the logarithm of the RRK law, eq 7[34])

$$\chi^2 = \sum_j \left(\frac{\ln k_0 - \dfrac{E_0'}{j} - \ln k^{j*}}{\Delta \ln k^{j*}} \right)^2 \tag{8}$$

where the term $E_0'/j \equiv (g - 1)E_0/(jh\nu)$ results from the first-order development of the logarithm and the denominator terms are the uncertainties on the measures. This χ^2 has a parabolic form in the [ln k_0, E_0] plane; thus, the terms of the Hessian error matrix are exact and the error contour is an ellipse (see Figure 7). This shape is actually found in our analysis (see Figure 8). The values of the parameters corresponding to the maximum likelihood are obtained by the first-order derivatives of χ^2. They take elegant compact forms

$$\ln k_0 = \frac{\sigma_{\ln k^{j*}/j,1/j} - \sigma_{\ln k^{j*},j^{-2}}}{\sigma_{1/j}^2} \tag{9}$$

$$E_0' = \frac{\sigma_{\ln k^{j*},j}}{\sigma_{1/j}^2} \tag{10}$$

where σ is the covariance[35] weighted by the $1/(\Delta \ln k^{j*})^2$. The second derivatives give the usual, one-dimension, error bars

$$\Delta_1 \ln k_0 = D \tag{11}$$

$$\Delta_1 E_0' = \sqrt{\langle j^{-2} \rangle}\, D \tag{12}$$

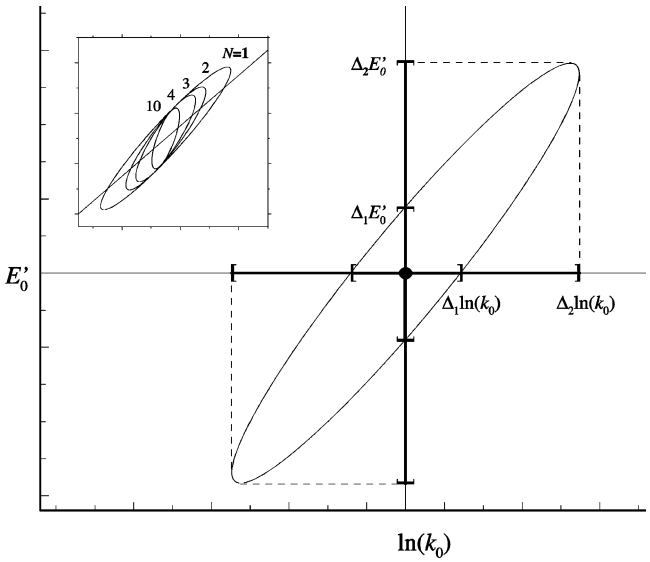

Figure 7. Ellipsoidal error contour in the two-dimensional case: all of the values of (ln k_0, E_0') such that the chi square is not greater than its minimum value plus one are included inside the ellipse. The bold segments correspond to the one- and two-dimension error bars. The incipit shows the shapes of the ellipses corresponding to 1, 2, 3, 4, and 10 absorbed photons in the case where all of the error bars on the k^{j*} are equal.

The uncertainty on one parameter is defined considering that the evaluation of the other parameter is exact. Thus, for example, $\chi^2(\ln k_0 \pm \Delta_1 \ln k_0, E_0') = \chi^2_{\min} + 1$ (see Figure 7). A more rigorous definition of the error bars consists of taking into account both uncertainties simultaneously. The two-dimension error bars are defined as the extend of the error contour given by $\chi^2 = \chi^2_{\min} + 1$. In our case the extreme points of the ellipse give

$$\Delta_2 \ln k_0 = \sqrt{\langle j^{-2} \rangle}\, \frac{D}{\sigma_{1/j}} \tag{13}$$

$$\Delta_2 E_0' = \frac{D}{\sigma_{1/j}} \tag{14}$$

Information on the distribution of the number of absorbed photons can be deduced from the slope and the lengthening of the ellipse:

$$\mathcal{S} \equiv \frac{\Delta_2 E_0'}{\Delta_2 \ln k_0} = \frac{\Delta_1 E_0'}{\Delta_1 \ln k_0} = \frac{1}{\sqrt{\langle j^{-2} \rangle}} \tag{15}$$

$$\mathcal{L} \equiv \frac{\Delta_2 E_0'}{\Delta_1 E_0'} = \frac{\Delta_2 \ln k_0}{\Delta_1 \ln k_0} = \frac{1}{\sqrt{1 - \dfrac{\langle j^{-1} \rangle^2}{\langle j^{-2} \rangle}}} \tag{16}$$

We stress the fact that the only ingredients of eqs 9−16 are the measures of k^{j*} and their error bars. They are independent of the way the measures were actually performed. Hence, these equations are valid in a large range of experimental studies.

Application to our Data. Our method of determination of the statistical law parameters did not consist of adjusting the laws to experimental measures of the k^{j*}. However, as can be seen in Figure 8, the resulting χ^2 actually shows an elliptic shape. Similar shapes are found for both statistical laws and both experiments. In this case very small one-dimension errors ($\Delta_1 \ln k_0 = 0.05$ and $\Delta_1 E_0 = 4 \times 10^{-3}$ eV) correspond to very

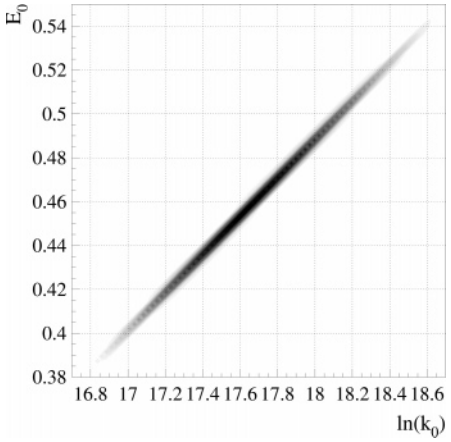

Figure 8. Experimental error contour corresponding to the 3.4 eV experiment adjusted by the RRK law.

large two-dimension errors ($\Delta_2 \ln k_0 = 0.85$ and $\Delta_2 E_0 = 8 \times 10^{-2}$ eV). Alternatively, if the value of E_0 can be faithfully determined by the theory, an experiment corresponding to a narrow error ellipse gives the value of k_0 with a low uncertainty.

The lengthening and the slope of this ellipse correspond to an intermediate case between $N = 1$ and $N = 2$ (see Figure 7). The application of eqs 15 and 16 gives $\langle j^{-1}\rangle^{-1} = \langle j^{-2}\rangle^{-1/2} = 1.9 \simeq 2$. This result confirms that, in the case of the second experiment, most fragmented cations have absorbed two photons, the other de-excitation yields play a negligible role. More generally, large lengthening will be found each time the uncertainty associated with one of the measurements is much smaller than the other uncertainties. Alternatively, the lengthening is reduced when constants corresponding to small as well as large numbers of absorbed photons are measured. However, in this case, the diminishing of the E_0 one-dimension error is negligible, as seen in Figure 7.

Appendix C: Verification of the Results Using the Signal Shape

The raw information delivered by the detector, located at the extremity of the time-of-flight arm, consists of time spectra in which amplitude is proportional to the molecular flow. In this paper, we have used a reduced form of the information, that is, the peak integrals, to determine the physical constants. In the following the coherence of the results with the signal shape will be verified.

Knowing the mechanical and electrical characteristics of the spectrometer, it is possible to calculate its transfer function and thus determine analytically the shape of the peaks corresponding to the molecules that have undergone fragmentation inside the electrical field.[26] In the case where the dissociation is driven by a single rate constant, the shape of the fragmentation peak depends on four inputs: (1) the shape of the parent molecule peak (which is obtained when the laser intensity is equal to zero), (2) the relative mass of the parent and fragmented molecules, (3) the rate constant of the dissociation, and (4) the proportion of excited parent molecules.

In the case of the $E_{\text{laser}} = 0.27$ mJ measurement, all of the detected fragmented molecules result from parent molecules excited by three photons (see Figure 5). The proportion of these excited molecules is 0.445, and the dissociation constant, as determined by the free adjustment, is 2.8×10^5 s^{-1}. The resulting curves are shown in Figure 9. The agreement with the detector signal is very good. The figure also shows the shape of the fragment peak (dashed line). About one-third of the peak

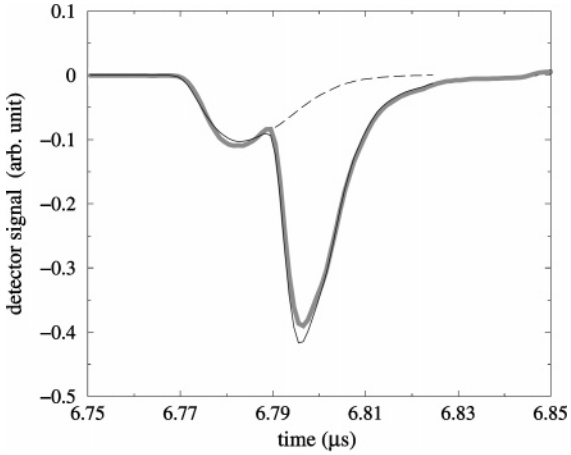

Figure 9. Comparison of the experimental (grey line) with the simulated (thin black line) detector signal profiles obtained for a laser energy of 0.27 mJ ($h\nu = 1.97$ eV). In this case all of the detected H-loss yield (dashed line) results from the absorption of three photons. The value of the dissociation constant k^{3*}_{-H} and the proportion of excited parent molecules were set to the values found by the free adjustment analysis.

corresponds to molecules that have broken up late in the acceleration zone of the spectrometer. Thus, they are screened in the parent peak.

References and Notes

(1) Léger, A.; Puger, J. *Astron. Atrophys.* **1984**, *137*, L5.
(2) Allamandola, L.; Tielens, A.; Barker, J. *Astrophys. J. Ser.* **1985**, *290*, L25.
(3) Sellgren, K. *Astrophys. J.* **1984**, *277*, 623.
(4) Moutou, C.; Verstraete, L.; Léger, A.; Sellgren, K.; Schmidt, W. *Astron. Astrophys.* **2000**, *354*, L17.
(5) Kerckhoven, C. V.; Hony, S.; Peeters, E.; Tielens, A.; Allamandola, L.; Hudgins, D.; Cox, P.; Roelfsema, P.; Voors, R.; Waelkens, C.; Waters, L.; Wesselius, P. *Astron. Astrophys.* **2000**, *357*, 1013.
(6) Proch, D.; Rider, D.; Zare, R. *Chem. Phys. Lett.* **1981**, *81*, 430.
(7) Boesl, U.; Neusser, H.; Weinkauf, R.; Schlag, E. *J. Phys. Chem.* **1982**, *86*, 4857.
(8) Kühlewind, H.; Neusser, H.; Schlag, E. *J. Phys. Chem.* **1984**, *88*, 6104.
(9) Kühlewind, H.; Kiermeier, A.; Neusser, H. *J. Chem. Phys.* **1986**, *85*, 4427.
(10) Kiermeier, A.; Ernstberger, B.; Neusser, H.; Schlag, E. *J. Phys. Chem.* **1988**, *92*, 3785.
(11) Neusser, H. *J. Phys. Chem.* **1989**, *93*, 3897.
(12) Rice, O.; Ramsperger, H. *J. Am. Chem. Soc.* **1928**, *50*, 617.
(13) Kassel, L. *J. Phys. Chem.* **1928**, *32*, 225.
(14) Léger, A.; Boissel, P.; Désert, F.; d'Hendecourt, L. *Astron. Atrophys.* **1989**, *213*, 351.
(15) Klippenstein, S.; Faulk, J. D.; Dunbar, R. *J. Chem. Phys.* **1993**, *98*, 243.
(16) Omont, A. *Astronom. Astrophys.* **1986**, *164*, 159.
(17) Barker, J. *Chem. Phys.* **1983**, *77*, 301.
(18) Tielens, A. G. G. M.; Allamandola, L. J.; Barker, J. R.; Cohen, M. *Polycyclic Aromatic Hydrocarbons and Astrophysics*; D. Reidel: Dordrecht, The Netherlands, 1987; p 273.
(19) Van-Oanh, N.-T.; Désesquelles, P.; Douin, S.; Bréchignac, P. *J. Phys. Chem. A* **2006**, *110*, 5592.
(20) This method is also the only one available to account for the time profile of the intensity of the laser pulse, when this profile has an influence on the results.
(21) For computer applications, the increment time must be very small with respect to all of the inverse rate constants. The results become stable when the time interval is smaller than a hundredth of the smallest inverse absorption or fragmentation constant.
(22) Because $n = (t_{\text{final}} - t_0)/\Delta t$ takes very large values, it is necessary, for numerical reasons and to keep a reasonable computing time, to solve this equation introducing $\mathscr{D}$, the matrix resulting from the diagonalization of $\mathscr{T}$, and $\mathscr{M}$, its modal matrix. The equation becomes $\mathbf{N}(t_f) = \mathscr{M}\mathscr{D}^n\mathscr{M}^{-1}\mathbf{N}(t_0)$. Thus, the matrix power is replaced by mere powers of reals.
(23) NAG. *NAG Fortran Library Routine Document*, first ed.; NAG: Oxford, U.K., 1997.

(24) Van-Oanh, N.-T.; Parneix, P.; Bréchignac, P. *J. Phys. Chem. A* **2002**, *106*, 10144.

(25) Nevertheless, as will be seen in the following, at high energy deposit the sensitivity of the experimental measurements to the dissociation scheme is limited. The right-hand cross sections are thus affected by large uncertainties.

(26) Van-Oanh, N.-T. *Spectroscopie et stabilité des hydrocarbures aromatiques polycycliques dans les conditions du milieu interstellaire* Ph.D. Thesis, Université Paris XI, 2003.

(27) Boissel, P.; Parseval, P.; Marty, P.; Lefèvre, G. *J. Chem. Phys.* **1997**, *106*, 4973.

(28) Ho, Y.; Dunbar, R.; Lifshitz, C. *J. Am. Chem. Soc.* **1995**, *117*, 6504.

(29) Szczepanski, J.; Dibben, M.; Pearson, W.; Eyler, J.; Vala, M. *J. Phys. Chem. A* **2001**, *105*, 9388.

(30) Pino, T.; Bréchignac, P.; Dartois, E.; Demyk, K.; d'Hendecourt, L. *Chem. Phys. Lett.* **2001**, *339*, 64.

(31) Jochims, H.; Rühl, E.; Baumgärtel, H.; Tobita, S.; Leach, S. *Astrophys. J.* **1994**, *420*, 307.

(32) Parneix, P.; Van-Oanh, N.-T.; Bréchignac, P. *Chem. Phys. Lett.* **2002**, *357*, 78.

(33) Van-Oanh, N.-T.; Parneix, P.; Bréchignac, P. *Chem. Phys. Phys. Chem.* **2006**, *7*, 1779.

(34) A slightly less straightforward calculation could be developed for the PTD law leading to the same qualitative conclusions.

(35) Noting $1/D^2 = \sum_j (1/(\Delta \ln k^{j^*})^2)$ the total weight, the weighted average of j^n is $\langle j^n \rangle = D^2 \sum_j (j^n/(\Delta \ln k^{j^*})^2)$, and the variance is $\sigma_{j^n}^2 = \langle j^{2n} \rangle - \langle j^n \rangle^2$.